

Approximation Schemes to Include Nuclear Motion in Laser-Driven Ab Initio Electron Dynamics: Application to High Harmonic Generation

Published as part of *The Journal of Physical Chemistry A virtual special issue "Attosecond Chemistry"*.

Paul Anton Albrecht,* Christoph Witzorky, Peter Saalfrank, and Tillmann Klamroth



Cite This: *J. Phys. Chem. A* 2023, 127, 5942–5955



Read Online

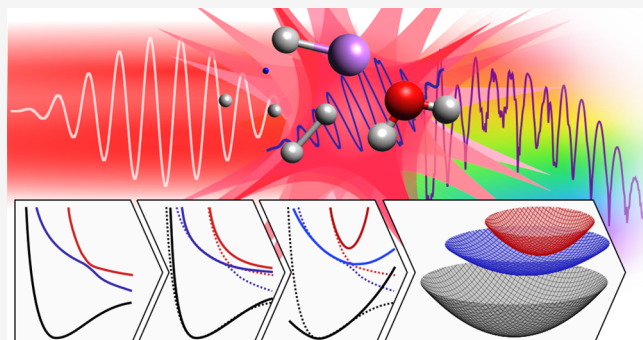
ACCESS |

Metrics & More

Article Recommendations

Supporting Information

ABSTRACT: The quantum mechanical description of many-electron dynamics in molecules driven by short laser pulses is at the heart of theoretical attoclassicality. In addition to the formidable time-dependent electronic structure problem, the field faces the challenge that nuclear motion, ideally also treated quantum mechanically, may not be negligible, but scales enormously in effort. As a consequence, most first-principles calculations on ultrafast electron dynamics in molecules are done within the fixed-nuclear approximation. For laser-pulse excitation in H_2^+ , where an “exact” treatment of the coupled nuclear-electron dynamics is possible, it has been shown that nuclear motion can have a nonnegligible impact on high harmonic generation (HHG) spectra (Witzorky *et al.*, *J. Chem. Theor. Comput.* 2021, 17, 7353–7365). It is not so clear, however, how to include (quantum) nuclear motion also for more complicated molecules, with more electrons and/or nuclei, in particular when the electronic structure is described by correlated, multistate wavefunction methods such as the time-dependent configuration interaction (TD-CI). In this work, we suggest a scheme in which the Born–Oppenheimer potential energy surfaces of a molecule are approximated by model potentials (harmonic and asymptotic, as an expansion in $1/R$), obtained from only a few ab initio calculations, with the prospect to treat complex molecular systems. The method is tested successfully for HHG by few-cycle laser pulses for the “exact” H_2^+ reference. It is then applied for diatomic molecules with more electrons and for a two-dimensional model of the water molecule using TD-CIS ($S = \text{single}$) for the electronic structure part.



1. INTRODUCTION

High harmonic generation (HHG) enables the creation of ultrashort laser pulses in the attosecond domain^{1–3} with variable photon energies up to soft X-rays.⁴ Corkum’s three-step model describes this process as the classical motion of an electron. First, the electron is set free through tunnel ionization and accelerated away from the parent ion; second, after half an optical cycle, it accelerates back; and third, it collides inelastically with the ion, resulting in the emission of photons with multiple frequencies of exciting light.⁵ The theoretical treatment of this process necessitates an accurate description of large-amplitude electron motion, as well as ionization during the HHG process. However, most calculations are done within a fixed-nuclei approximation; it was shown in a recent work for H_2^+ ^{6–9} that nuclear motion can have a significant influence on HHG intensities. While HHG involves usually no bond-breakings and bond formation in molecules, it is still at the heart of attoclassicality and the question arises, how for HHG and related phenomena induced by ultrashort laser pulses,

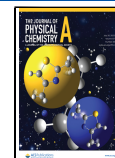
nuclear motion can be included on top of the explicit treatment of ultrafast electron dynamics.

The quantum treatment of coupled electronic and nuclear motion has been accomplished for very small molecules, like H_2^+ or related species, by numerically solving the molecular time-dependent Schrödinger equation on extended grids, among other things also in order to describe HHG.^{6,7,9–11} The general attention, however, has shifted from small molecules^{6,12–14} to larger ones^{15–23} recently. Chemically interesting molecules beyond H_2^+ or alike are out of reach for the full solution of the coupled nuclear-electronic time-dependent Schrödinger equations. Hence, approximate methods are needed for many-electron systems.

Received: March 17, 2023

Revised: June 19, 2023

Published: July 7, 2023



Strong advances have been made in this direction with real-time time-dependent density functional theory (RT-TD-DFT).^{24–26} There, nuclear motion is usually treated in classical approximation via a time-dependent potential felt by the electrons. Therefore, the method does not treat nuclear motion quantum mechanically on multistate potentials.

Other methods are based on wavefunction theory (WFT) and are systematically improvable, such as the multi-configurational expansion of the total wavefunction for electron-nuclear dynamics (MCEND)^{27–31} and the nuclear-electron orbitals (NEO) method. The latter treats electrons and selected nuclei (typically protons) quantum mechanically and uses various WFT methods for the former^{32,33} (within NEO, the electronic problem can also be tackled by DFT, NEO-DFT³⁴). Nuclear motion has been included for H_2^+ and H_2 (on a grid in one dimension³⁵ or using MCTDHF^{36,37}). Bigger molecules as LiH were treated in ref 31, however, without taking ionization and long-amplitude electron motion into account. Still, these WFT methods are currently limited to few-body problems in practice.

Yet, established comparisons are done for the H_2^+ model problem. We note that the coupled electron-nuclear problem can not only be solved on (extended) grids for all (three) degrees of freedom but also by using a standard Gaussian-type orbital basis, computing potential energy curves and describing only the nuclear wavepacket motion by grid methods. This approach was used in ref 9, where it was also shown that nuclear motion had a clear effect on HHG as just mentioned. Non-Born–Oppenheimer transitions between the many different potential energy surfaces via kinetic coupling terms in the coupled nuclear Schrödinger equation were also included, but found to be unimportant for the specific case studied in ref 9, namely, HHG following nonresonant (800 nm) laser-pulse excitation of H_2^+ in its electronic ground state. (For other scenarios, e.g., muonic analogues of H_2^{11} or for optically preexcited molecules, nonadiabatic couplings (NACs) can be more important.) Gaussian bases for the electronic structure part have the big advantage of being readily available and flexible, even for large-amplitude electronic motion, and can be used in a highly efficient manner also for many-electron systems in the context of correlated WFT, e.g., for time-dependent configuration interaction (TD-CI),^{38–42} multi-configurational time-dependent Hartree–Fock (MCTDHF),^{36,37,43–46} or time-dependent coupled-cluster (TD-CC)^{47,48} methods. Because the computation of potential energy curves or multidimensional potential energy surfaces (and their nonadiabatic couplings) is very cumbersome, in particular if a multitude of them is needed (e.g., after excitation with ultrashort laser pulses), correlated TD-WFT including nuclear motion has hardly been used and often the fixed-nuclei approximation was adopted instead.

To make progress toward quantum nuclear motion also for TD-WFT methods, approximations for the potential energy curves/surfaces (and, possibly, also for NACs) and transition dipole moments are needed, which are accurate enough to describe the basic physics but nevertheless are easily accessible by, e.g., only few-point, standard ab initio calculations. To suggest and test such approximations is a central goal of this paper. Two approximations will be tested for potential curves, a “harmonic” approximation and an “asymptotic” approximation (to account for dissociative states). For transition dipole moments, constant (“Condon”) and linear (“Herzberg–Teller”) approximations will be tested. Here, we restrict

ourselves mostly to diatomic molecules, i.e., to potential and dipole curves, and we neglect non-Born–Oppenheimer terms for the time being. However, the approach opens the way also to more complicated situations, and this will be demonstrated for one example, namely, HHG for a water molecule, treated in a reduced (two-mode) model and using potential energy surfaces in harmonic approximation.

Note that in effect, we suggest an approximate treatment of nonadiabatic dynamics and spectroscopy similar in spirit to the celebrated vibronic coupling model⁴⁹ (used for both photochemistry and spectroscopy), or by harmonic models for spectroscopy, e.g., the independent mode displaced harmonic oscillator (IMDHO) model (with or without frequency alteration and/or Duschinsky rotation).⁵⁰ In these models, however, typically only one or few excited states are involved, while here many of them will be considered.

The two approximation schemes are compared in detail to previous results using WFT with Gaussian-type orbitals, of the laser-driven, coupled nuclear-electronic problem for H_2^+ . In addition, we apply our approximations for the diatomic molecules H_2 and LiH as two- and four-electron systems, respectively, with the electronic part treated by the configuration interaction singles (CIS) method.⁵¹ Finally, we also study, by the same method, HHG in H_2O , using a harmonic two-mode model for the high-frequency stretching O–H vibrations at a fixed H–O–H bond angle. Note that the suggested approximations can describe nuclear motion also for other approaches obtained from a linear response TD-DFT.^{52,53}

The paper is organized as follows. In Section 2, we reiterate the basics of laser-driven coupled nuclear-electron quantum dynamics, including the computation of HHG spectra. Section 3 introduces approximations adopted in this work for potential surfaces and dipole functions. In Section 4, we present the results, first for the test system, H_2^+ (Section 4.1), and then for the other diatomic molecules studied in this work (Section 4.2). The water molecule as an example for a polyatomic system is studied in Section 4.3. The final Section 5 concludes our work. Atomic units $4 \pi e_0 = \hbar = e = m_e = 1$ are used everywhere, if not mentioned otherwise.

2. THEORY

2.1. Laser-Driven Coupled Nuclear-Electron Dynamics.

In what follows, we solve the molecular, time-dependent Schrödinger equation (TDSE)

$$i \frac{\partial \Psi(\underline{r}, \underline{R}; t)}{\partial t} = \hat{H}(t) \Psi(\underline{r}, \underline{R}; t) \quad (1)$$

Here, $\underline{r} = (r_1, \dots, r_N)$ are spatial coordinates of N electrons (spin coordinates not noted here), $\underline{R} = (R_1, \dots, R_M)$ those of M nuclei, and $\hat{H}(t)$ specifies the system Hamiltonian with a laser coupled to the molecule, modeled in the semiclassical dipole approximation, as

$$\hat{H}(t) = \hat{H}_0 - \hat{\mu} \underline{E}(t) \quad (2)$$

In eq (2), \hat{H}_0 is the field-free molecular Hamiltonian

$$\hat{H}_0 = \hat{T}_n + \hat{T}_e + \hat{V}_{nn} + \hat{V}_{ne} + \hat{V}_{ee} = \hat{T}_n + \hat{H}_e \quad (3)$$

with $\hat{T}_n = -\sum_{A=1}^M \frac{1}{2M_A} \Delta_A$ and $\hat{T}_e = -\frac{1}{2} \sum_{i=1}^N \Delta_i$ being kinetic energy operators of nuclei (masses $\{M_A\}$) and electrons, respectively. $\hat{V}_{nn} = \sum_{A=1}^M \sum_{B>A}^M \frac{Z_A Z_B}{|\underline{R}_A - \underline{R}_B|}$ is the internuclear

repulsion ($Z_{A/B}$ are nuclear charges), $\hat{V}_{en} = -\sum_{A=1}^M \sum_{i=1}^N \frac{Z_A}{|\underline{R}_A - \underline{r}_i|}$ the nuclear-electron attraction, and $\hat{V}_{ee} = \sum_{i=1}^N \sum_{j>i}^N \frac{1}{|\underline{r}_i - \underline{r}_j|}$ the interelectronic repulsion potential.

In eq 3, we combined the last four terms in that equation in the field-free electronic Hamiltonian, \hat{H}_e , which satisfies the electronic Schrödinger equation

$$\hat{H}_e \psi_j(\underline{r}; \underline{R}) = V_j(\underline{R}) \psi_j(\underline{r}; \underline{R}) \quad (4)$$

with potential energy surfaces, $V_j(\underline{R})$, and electronic wavefunctions, $\psi_j(\underline{r}; \underline{R})$, for state j .

The molecule-laser coupling is described by the term $-\hat{\mu}E(t)$ in eq 2. The time-dependent electric field $E(t)$, independent of coordinates in dipole approximation, is chosen as

$$E(t) = E_0 \underline{P} s(t) \cos(\omega_0(t - t_p)) \quad (5)$$

with the polarization vector \underline{P} , the carrier frequency ω_0 , and a \cos^2 envelope

$$s(t) = \begin{cases} \cos^2\left(\frac{\pi}{2\sigma_p}(t - t_p)\right), & \text{if } |t - t_p| \leq \sigma_p \\ 0, & \text{else} \end{cases} \quad (6)$$

$2\sigma_p$ denotes the pulse duration and t_p the peak time with maximal amplitude of the laser, E_0 . We chose $t_p = 2\sigma_p$ for an even-centered pulse. Further, $\hat{\mu}$ is the molecular dipole operator, $\hat{\mu} = -\sum_{i=1}^N \underline{L}_i + \sum_{A=1}^M Z_A \underline{R}_A$.

2.2. Nuclear Motion in Born–Oppenheimer Representation. For small systems (like H_2^+), eq (1) can be solved directly on a three-dimensional grid, and HHG spectra for H_2^+ have been provided in ref 9 by this “all-grid” method. Alternatively, the coupled nuclear-electron dynamics can be described by expressing the wavefunction within the Born–Huang ansatz⁵⁴

$$\Psi(\underline{r}, \underline{R}; t) = \sum_j \psi_j(\underline{r}; \underline{R}) \Phi_j(\underline{R}; t) \quad (7)$$

with j the adiabatic, electronic-state index. Multiplying the TDSE with ψ_i^* from the left, integrating over electron coordinates, \underline{r} , and obeying the orthogonality relation $\langle \psi_i | \psi_j \rangle_{\underline{r}} = \delta_{ij}$, leads to

$$i \frac{\partial}{\partial t} \Phi_i(\underline{R}; t) = \sum_j \hat{H}_{ij}(t) \Phi_j(\underline{R}; t) \quad (8)$$

with Hamiltonian matrix elements

$$\begin{aligned} \hat{H}_{ij}(t) &= \langle \psi_i | \hat{H}(t) | \psi_j \rangle_{\underline{r}} \\ &= (\hat{T}_n + V_i(\underline{R})) \delta_{ij} - \hat{\mu}_{ij}(\underline{R}) E(t) + \hat{D}_{ij} \end{aligned} \quad (9)$$

Here, $\hat{\mu}_{ij}(\underline{R}) = \langle \psi_i | \hat{\mu} | \psi_j \rangle_{\underline{r}}$ are transition dipole moments connecting states i and j (if $i \neq j$) and permanent dipole moments $\hat{\mu}_{jj}(\underline{R})$ (if $i = j$), respectively. The \hat{D}_{ij} are non-Born–Oppenheimer coupling terms ($i \neq j$) and diagonal non-Born–Oppenheimer terms ($i = j$), respectively, defined in ref 9. At least for situations considered here, HHG emitted from molecules initially in their ground state, where conical intersections are typically not reached and nonadiabatic

transitions do not occur. Therefore, the nonadiabatic coupling terms are of minor importance,⁹ and are therefore neglected. This constitutes the Born–Oppenheimer approximation, which we use for all multistate models to be considered below.

In this paper, we mostly consider diatomic molecules $A-B$ and a polarization of the laser pulse along the molecular axis is assumed, i.e., nuclear motion is only along the distance coordinate, $R = |\underline{R}_A - \underline{R}_B|$, $\hat{T}_n = -\frac{1}{2m} \frac{\partial^2}{\partial R^2}$ (with $m = M_A M_B / (M_A + M_B)$ being the reduced nuclear mass), and $\mu_{ij}(R) E(t) = \mu_{ij}(R) E(t)$.

2.3. High Harmonic Generation Spectra. In what follows, we calculate high-harmonics spectra from Fourier transformed dipole acceleration functions

$$I(\omega) \propto \left| \int_0^{t_f} w(t) e^{-i\omega t} \left(\frac{d^2 \mu_z(t)}{dt^2} \right) dt \right| \quad (10)$$

Here, for diatomic molecules, $\mu_z(t) = \langle \Psi(\underline{r}, R; t) | \hat{\mu}_z | \Psi(\underline{r}, R; t) \rangle_{\underline{r}, R}$ is the molecular dipole moment along the molecular axis, z . The laser was assumed to be directed along the molecular axis, aligning z with R . Further, a Hann window $w(t) = \sin^2(\pi t/t_f)$ was used to reduce noise in the simulated spectrum. We integrate up $t_f = 2\sigma_p$, the pulse duration (pulse parameters given in Section 3.1). Additionally, in the multisurface models, R -dependent HHG spectra were calculated by evaluating dipole time derivatives as a function of R

$$I(R; \omega) \propto \left| \int_0^{t_f} w(t) e^{-i\omega t} \left(\frac{d^2 \mu_z(R; t)}{dt^2} \right) dt \right| \quad (11)$$

with $\mu_z(R; t) = \langle \Psi(\underline{r}, R; t) | \hat{\mu}_z | \Psi(\underline{r}, R; t) \rangle_{\underline{r}}$. Finally, we also estimated time-resolved HHG spectra, by time-windowed Fourier transformations of the dipole acceleration, as

$$I(t; \omega) \propto \left| \int_0^{t_f} w(t') e^{-i\omega t} \left(\frac{d^2 \mu_z(t')}{dt'^2} \right) g(t' - t) dt' \right| \quad (12)$$

Here, $g(t' - t)$ is a unit step function, $400 \frac{\hbar}{E_h}$ wide, centered at t .

Possible ionization losses were included in the dynamics (see Section 2.4) and the wavefunction was not renormalized for the calculation of dipole moments or HHG spectra.

2.4. Treatment of Ionization Losses. The interaction of intense laser pulses with the molecule leads to HHG and also to partial ionization. To account for ionization losses within multistate models, eq 8, an imaginary term was added, for H_2^+ , to the electronic potential $V_j(R)$, $V_j(R) \rightarrow V_j(R) - \frac{i}{2} \Gamma_j(R)$, with

$$\Gamma_j(R) = \begin{cases} 0, & \text{if } E_{e,j}(R) < 0 \\ \frac{\sqrt{E_{e,j}(R)}}{d}, & \text{else} \end{cases} \quad (13)$$

being the loss rate, for state j ($-i\frac{\hbar}{2} \Gamma_j$ would be an imaginary potential, and in atomic units $\hbar = 1$). Here, $E_{e,j}(R)$ is the excess energy of the electron above the ionization potential, i.e., $E_{e,j}(R) = V_j(R) - V_{nn}(R)$ (with $V_{nn}(R)$ the nuclear repulsion), and d is an “escape length” beyond which the electron is considered as free. This model⁹ generalizes a heuristic

ionization model originally developed for fixed-nuclei multistate models,⁵⁵ to the case when the electronic states become potential energy surfaces or potential curves, giving $E_{e,j}(R) = V_j(R) - \frac{1}{R}$ for H_2^+ . For H_2 , LiH, and also H_2O , however, we neglected the coordinate dependence of Γ_j and computed rates from virtual Hartree–Fock orbital energies, $E_{e,j} \rightarrow \varepsilon_r$, evaluated at the ground-state equilibrium geometries, i.e., we used the heuristic ionization model for fixed-nuclei multistate cases of ref 55. The escape length was chosen as $d = 1a_0$ throughout. In ref 9, also higher values of d were tested for H_2^+ . Despite some improvements for the intensity of some harmonics, the ionization rate decreases and creates more noise.

3. “EXACT” AND “APPROXIMATE” SOLUTIONS OF THE ELECTRON-NUCLEAR SCHRÖDINGER EQUATION

In this section, we provide more details, also numerical, on the “exact” solution (without non-Born–Oppenheimer terms) of the multistate TDSE (eq 8) (Section 3.2), and we suggest approximate schemes that largely avoid costly evaluations of full potential energy and (transition) dipole surfaces along the nuclear coordinates (Section 3.3). The “exact” scheme was used for H_2^+ , while the approximate schemes (with “harmonic” and “asymptotic” potential approximations, see below) were applied to H_2^+ , H_2 , and LiH. For the H_2O two-mode model, only the “harmonic” approximation was applied.

3.1. Pulse Parameters. Similar laser pulses were used for all calculations. Specifically, a frequency of $\omega_0 = 0.056954 \frac{\text{E}_h}{\text{h}}$ (corresponding to a wavelength of 800 nm) was chosen with field amplitudes E_0 of 0.03, 0.09, and $0.15 \frac{\text{E}_h}{ea_0}$, corresponding to intensities of 3.16×10^{13} , 2.84×10^{14} , and $7.90 \times 10^{14} \frac{\text{W}}{\text{cm}^2}$, respectively. For H_2O , a field amplitude of $E_0 = 0.04 \frac{\text{E}_h}{ea_0}$ was chosen with intensity $5.62 \times 10^{13} \frac{\text{W}}{\text{cm}^2}$. The pulse duration t_f was set to 10 cycles, giving $t_f = 2\sigma_p = 2t_p = 1103.2 \frac{\text{h}}{\text{E}_h}$ (or 26.69 fs). The pulse was polarized along the molecular axis. Pulse parameters for H_2^+ are the same as in ref⁹, making our results directly comparable to the results there.

3.2. “Exact” Solution of the Multistate TDSE. In this section, we refer to the diatomics only. Numerical details for H_2O will be described in Section 4.3. To solve the nuclear Schrödinger equation (eq 8), matrix elements \hat{H}_{ij} are needed for which the electronic Schrödinger equation (eq 4) must be solved. Also, the nuclear wavepackets need to be propagated on the manifold of potential energy surfaces $\{V_j(R)\}$.

3.2.1. Nuclear Dynamics. As for the latter, a grid method was used, which is described in ref 9. That is, the nuclear wavefunctions $\Phi_j(R, t)$ are represented on an equidistant R -grid, and Fast Fourier Transform (FFT) techniques are applied to represent kinetic and potential terms in local representations. For H_2^+ , 192 grid points were used, starting at $0.12a_0$ and ending at $15.4a_0$ with a grid spacing of $dR = 0.08a_0$.⁹ In addition to “exact” potential curves, also approximate potential curves were employed: “harmonic” and “asymptotic” ones (see below). For H_2 and LiH, where only these approximate forms were used, the grids were $[-3.24a_0, 7.0a_0]$ over 128 points ($dR = 0.08a_0$) for the “harmonic” H_2 system, $[0.12a_0, 10.36a_0]$ ($dR = 0.08a_0$) for the “asymptotic” H_2 system, and $[0.12a_0,$

$15.54a_0]$ ($dR = 0.015a_0$) over 1028 points for LiH in both approximations.

Imaginary absorbers and flux analysis were used at grid boundaries to analyze dissociating molecules; however, dissociation played practically no role up to the final propagation time used here. The time propagation was done with a Runge–Kutta scheme of fourth order up to a final propagation time, t_f , with a time step of $\Delta t = 0.02 \frac{\text{h}}{\text{E}_h}$. In the coupled-surface approach, initial nuclear-electronic wavefunctions were prepared by imaginary-time propagation, in the electronic ground state of the adiabatic, field-free Hamiltonian.

3.2.2. Electronic Structure Problem. Regarding the electronic structure problem, for H_2^+ , the same techniques as in ref 9 were applied. That is, “exact” electronic potentials $V_j(R)$, dipole moments $\mu_{ij}(R)$, and adiabatic electronic wavefunctions $\psi_j(r; R)$ were calculated by solving eq (4) using the Gaussian-type orbital basis aug-cc-pVTZ,⁵⁶ with additional first eight so-called Kaufmann shells⁵⁷ with halved exponents (see ref 9 for further details). This basis set is very diffuse and particularly suited for large-amplitude motion of the electron, as it occurs during HHG. Using the grid representation for nuclei and the Gaussian basis set approach, all for solving (eq 8), with non-Born–Oppenheimer terms neglected, will also be referred to below as the “exact Born–Oppenheimer” solution. Using larger basis sets only moderately improves computed HHG spectra, but—at the same time—leads to numerical problems, due to very small eigenvalues of the overlap matrix.

For H_2 and LiH, with two and four electrons, respectively, we will solve the Born–Oppenheimer TDSE (eq 8) by still using the grid method for the nuclear part, while the electronic Schrödinger equation will be solved by the CIS method but at selected points along R only that are needed to create approximate, “harmonic” and “asymptotic” potential energy curves, $V_j(R)$, and dipole functions, $\mu_{ij}(R)$, respectively (see Section 3.2). Specifically, the CIS calculations were based on Hartree–Fock calculations done with Psi4,⁵⁸ with the aug-cc-pVTZ basis set and additionally the unaltered first eight Kaufmann shells placed at the center of mass of the molecules.

3.3. “Approximate” Potential and Dipole Functions for the Multistate TDSE. As said, in this work, we develop approximate schemes for computing potential energy curves and transition dipole moments for H_2^+ , H_2 , and LiH (and H_2O), determined from few ab initio calculations only. Two main approximations will be used below for potential curves $V_j(R)$ and then adopted in eq 8, called the “harmonic approximation” and the “asymptotic approximation”, respectively. Also, two approximations for (transition) dipole moments $\mu_{ij}(R)$ will be tested, namely, the “Condon approximation” ($\mu_{ij} = \text{const.}$) or the “linear” (or “Herzberg–Teller”) approximation (see below). As a third, more drastic approximation, we also performed “fixed-nuclei” calculations for all molecules.

3.3.1. Approximate Potential Energy Curves. **3.3.1.1. Harmonic Approximation.** In the harmonic potential approximation, we approximate all potential curves, $V_j(R)$, by harmonic oscillator potentials, obtained from a second-order Taylor expansion around a reference point, R_0 , as

$$V_j^{\text{HO}}(R) = A_j(R - R_{\min,j})^2 + E_{\min,j} \quad (14)$$

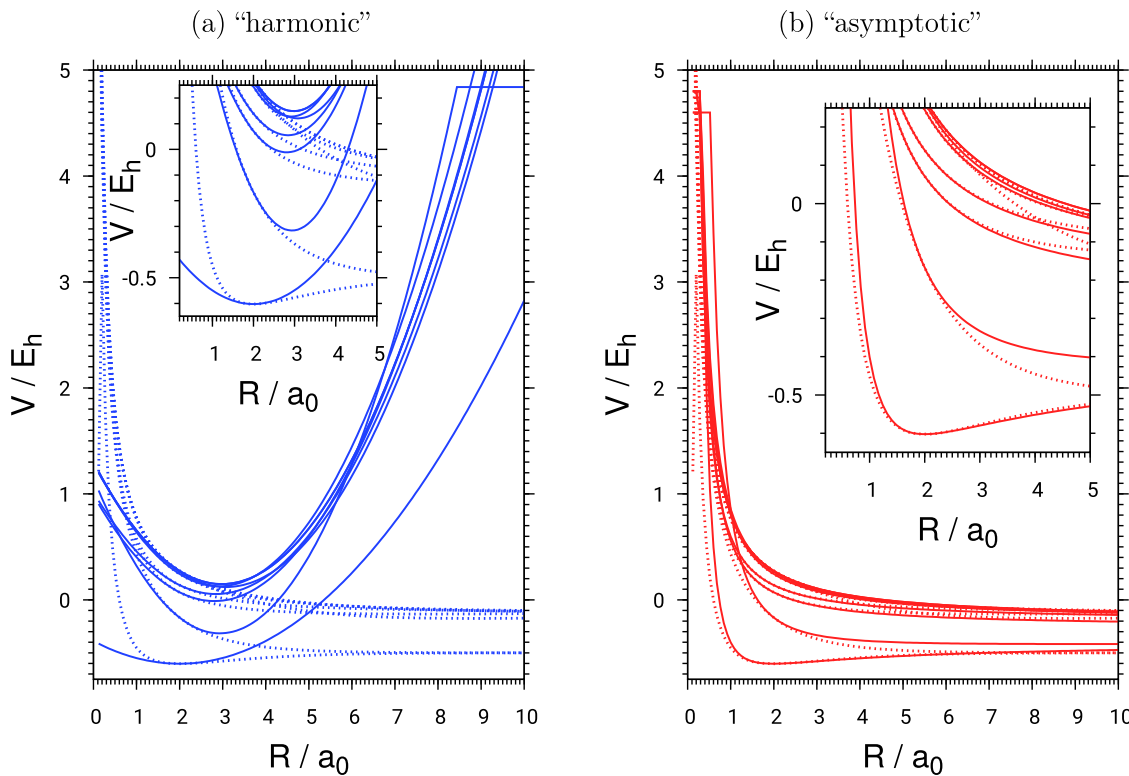


Figure 1. Exact potentials of the eight lowest lying electronic states of H_2^+ (dotted) and corresponding harmonic (straight lines (a)) and asymptotic fits (straight lines (b)). Insets show enlarged areas.

Here, as shown in [Appendix A](#), $A_j = \frac{1}{2}V''(R_0)$, $R_{\min,j} = [R_0 - V'_j(R_0)/V''(R_0)]$, and $E_{\min,j} = [V_j(R_0) - V'_j(R_0)^2/(2V''(R_0))]$. Therefore, what is needed are the potential at the reference point, R_0 , $V_j(R_0)$, the first derivative of V_j at that point, $V'_j(R_0)$, and the second derivative at this point, $V''_j(R_0)$. The first and second derivatives are calculated from three-point formulas as shown in [Appendix B](#), requiring $V_j(R_0)$, $V_j(R_0 + \Delta R)$, and $V_j(R_0 - \Delta R)$, where ΔR is a displacement from the reference point.

For H_2^+ , $R_0 = 1.98a_0$ was chosen rather than the computed ground-state equilibrium distance of $1.9994a_0$ calculated with the basis set mentioned above. (This small deviation from the ground-state minimum had almost no effect on the potential curves but avoided numerical instabilities shown in [Figure S2](#).) For H_2 and LiH , where the CIS method was employed, R_0 , chosen as the Hartree–Fock equilibrium distances without Kaufmann functions of the ground state (corresponding to the CIS), was adopted with $R_0 = 1.388a_0$ for H_2 and $R_0 = 3.038a_0$ for LiH , respectively. The displacement for obtaining derivatives was chosen as $\Delta R = 0.001a_0$ after convergence tests as described in [Appendix B](#). For propagations, also cutoff criteria for the potentials were employed at very high energies (above $5E_h$ above $E_{\min,j}$). Further slight adjustments to avoid numerical instabilities are also described in [Appendix A](#).

For H_2^+ , the lowest “exact” and harmonically approximated potentials $V_j(R)$ and $V_j^{\text{HO}}(R)$ are compared in [Figure 1a](#). Note that the harmonic potentials are shifted and they have different force constants, i.e., they go beyond the simple displaced-oscillator approximation.

3.3.1.2. Asymptotic Approximation. In order to improve beyond the harmonic approximation, higher-order derivatives could be included in the Taylor expansion of the potential curves. Here, instead, we adopt an “asymptotic approximation”

by expanding V_j in a series in $1/R$ and truncating after the quadratic term, as

$$V_j^{\text{asym}}(R) = B_{0,j} + B_{1,j} \frac{1}{R} + B_{2,j} \left(\frac{1}{R}\right)^2 \quad (15)$$

This expansion is justified in [Appendix C](#), where also the parameters $B_{0,j}$, $B_{1,j}$, and $B_{2,j}$ are defined and other details are given. It provides a more realistic representation of molecular potential energy curves with origins going back to the 1920s.^{59,60} The evaluation of parameters $B_{n,j}$ requires, again, a reference distance R_0 , and the potential V_j and first and second derivatives of V_j at R_0 . The same R_0 was used as above. The asymptotic potentials account for bound and unbound potential curves, with a finite dissociation energy. If the nuclear wavepacket moves toward large R -values, this may or may not have an impact on computed properties, like HHG signals. Again, an energy cutoff ($>5 E_h$ above the dissociation energies predicted by the asymptotic form) was introduced.

For H_2^+ , the lowest eight “exact” and asymptotically approximated potentials $V_j(R)$ and $V_j^{\text{asym}}(R)$ are compared in [Figure 1b](#). It can be recognized that, trivially, the potential curves are better represented by $V_j^{\text{asym}}(R)$ than by $V_j^{\text{HO}}(R)$. Looking more closely, the low dissociation energy of H_2^+ leads to strong anharmonicity of the ground-state potential, for example, resulting in a bad fit with the harmonic approximation. The asymptotic potential approximation fits the exact potential better, but there are still significant differences: At small R , the exact ground-state potential is dominated by the nuclear repulsion $V_{nn}(R) = \frac{1}{R}$, whereas the approximation is dominated by $\frac{1}{R^2}$. Additionally, the exact potential has a slightly different dissociation energy.

3.3.2. Approximate (Transition) Dipole Moments. Also, (transition) dipole moments were approximated. Constant (Condon approximation) and linear approximations (Herzberg–Teller approximation)⁶¹ in R were tested

$$\mu_{ij}^{\text{HT}}(R) = \mu'_{ij}(R_0)(R - R_0) + \mu_{ij}(R_0) \quad (16)$$

where $\mu'_{ij}(R_0)$ denotes the derivative of μ_{ij} at R_0 and $\mu_{ij}(R_0)$ its corresponding value there. For the calculation of the dipole gradients, $\mu'_{ij}(R_0)$, an adiabatic connection scheme was used, as described in ref 9. For the linear approximation of the dipole moments, a cutoff at $\pm 0.5a_0e$ to the original dipole at R_0 was introduced. Both dipole approximations gave similar results for signal shapes but slightly higher peak intensity for Herzberg–Teller, more comparable to intensities obtained with exact dipoles. Below, if not explicitly stated otherwise, the Herzberg–Teller approximation will be used.

4. RESULTS AND DISCUSSION

4.1. “Exact” and “Approximate” HHG Spectra for H_2^+ .

4.1.1. Test of Approximations. We first of all compare, in Figure 2, for various laser-pulse intensities, the HHG spectra of H_2^+ , obtained with various methods:

- by solving the multistate TDSE for the nuclei using “exact” potential curves $V_i(R)$ and (transition) dipole moments $\mu_{ij}(R)$ but neglecting non-Born–Oppenheimer terms—this is termed “Born–Oppenheimer” (BO) in the figure;
- by solving the multistate TDSE with “harmonically approximated” potentials (and dipoles in Herzberg–Teller approximation)—“harmonic approximation” in the figure;
- by solving the multistate TDSE with “asymptotically approximated” potential curves (and dipoles in HT approximation)—“asymptotic approximation” in the figure.

In all cases, 118 states were considered, as in ref 9. In ref 9, also a comparison of the “all-grid” solution to the multistate model with and without nonadiabatic couplings was provided. At low and medium field intensities, only moderate differences between “all-grid” and multistate models for HHG spectra of H_2^+ occur, which are mainly due to different numerical settings as argued in ref 9. At a high intensity, larger differences emerge, probably because of high ionization losses and their different treatment. Instead, we shall consider the “exact Born–Oppenheimer” method as a reference for judging the approximate methods.

From Figure 2, we note the following. The “exact BO” solutions (black curves), already presented in ref 9 for the same laser pulses, show the typical characteristics of homonuclear diatomic molecules, i.e., odd harmonics only with three regimes: A high-peak intensity region with a rapid falloff for low harmonics, a broad plateau region for intermediate harmonics, and a cutoff region for the highest harmonics. Onset and end of the plateau region depend on the laser intensity, for instance, the cutoff onset being a linear function of the intensity $I \propto E_0^2$ according to Corkum’s three-step model.⁵

Comparing harmonically (blue lines) and asymptotically (red) approximated spectra in Figure 2 with the “exact Born–Oppenheimer” solutions, we note that the overall trends and basic features of the “exact” reference are well reproduced by

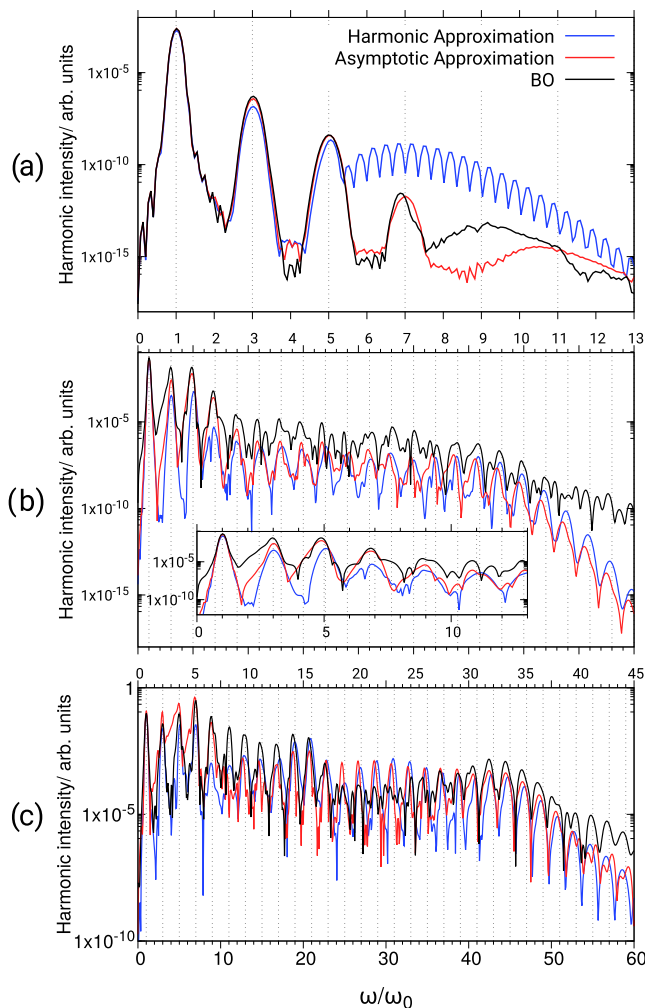


Figure 2. Comparison of HHG spectra of H_2^+ , obtained with laser field amplitudes of $E_0 = 0.03 \frac{E_h}{ea_0}$ (a), $E_0 = 0.09 \frac{E_h}{ea_0}$ (b), and $E_0 = 0.15 \frac{E_h}{ea_0}$ (c) of an 800 nm, 10-cycle pulse. “Exact Born–Oppenheimer” (“BO”) solutions are shown in black, curves in “harmonic approximation” in blue, and curves in “asymptotic approximation” in red. The y -axis shows logarithmic HHG intensities in arbitrary units, the x -axis gives the harmonic order, i.e., ω/ω_0 .

the approximate methods. For $E_0 = 0.03 \frac{E_h}{ea_0}$, they agree almost perfectly for the lowest three peaks, except the harmonic approximation having slightly lower intensities for the third and fifth harmonic. At medium laser intensity ($E_0 = 0.09 \frac{E_h}{ea_0}$), this underestimation of HHG intensities is more pronounced and uniform over the entire emission range. (At the very highest laser intensity ($E_0 = 0.15 \frac{E_h}{ea_0}$), the situation is less uniform.) Generally, the agreement between “exact” and “approximate” HHG spectra is quantitatively less convincing for very high harmonics, notably beyond the cutoff.

When comparing both approximations, “harmonic” and “asymptotic”, we note that they also agree reasonably well with each other particularly at higher laser intensities (Figure 2b,c), but also some differences between them emerge. First, artifacts beyond the fifth harmonic appear in the harmonic case for the lowest intensity (Figure 2a). This behavior can be traced back to a resonance feature, involving the first excited state, which is unbound and therefore poorly described in the harmonic

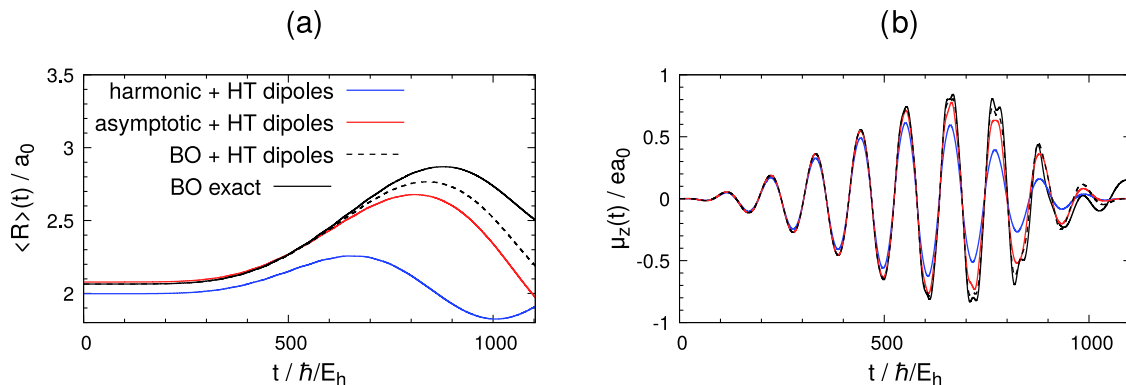


Figure 3. Comparison of expectation values $\langle R \rangle(t)$ (a) and dipole moments $\mu_z(t)$ for H_2^+ (b), obtained with different multistate models, “BO exact”, and approximations thereof (see text), for a 10-cycle laser pulse, 800 nm, $E_0 = 0.09 E_h/(ea_0)$.

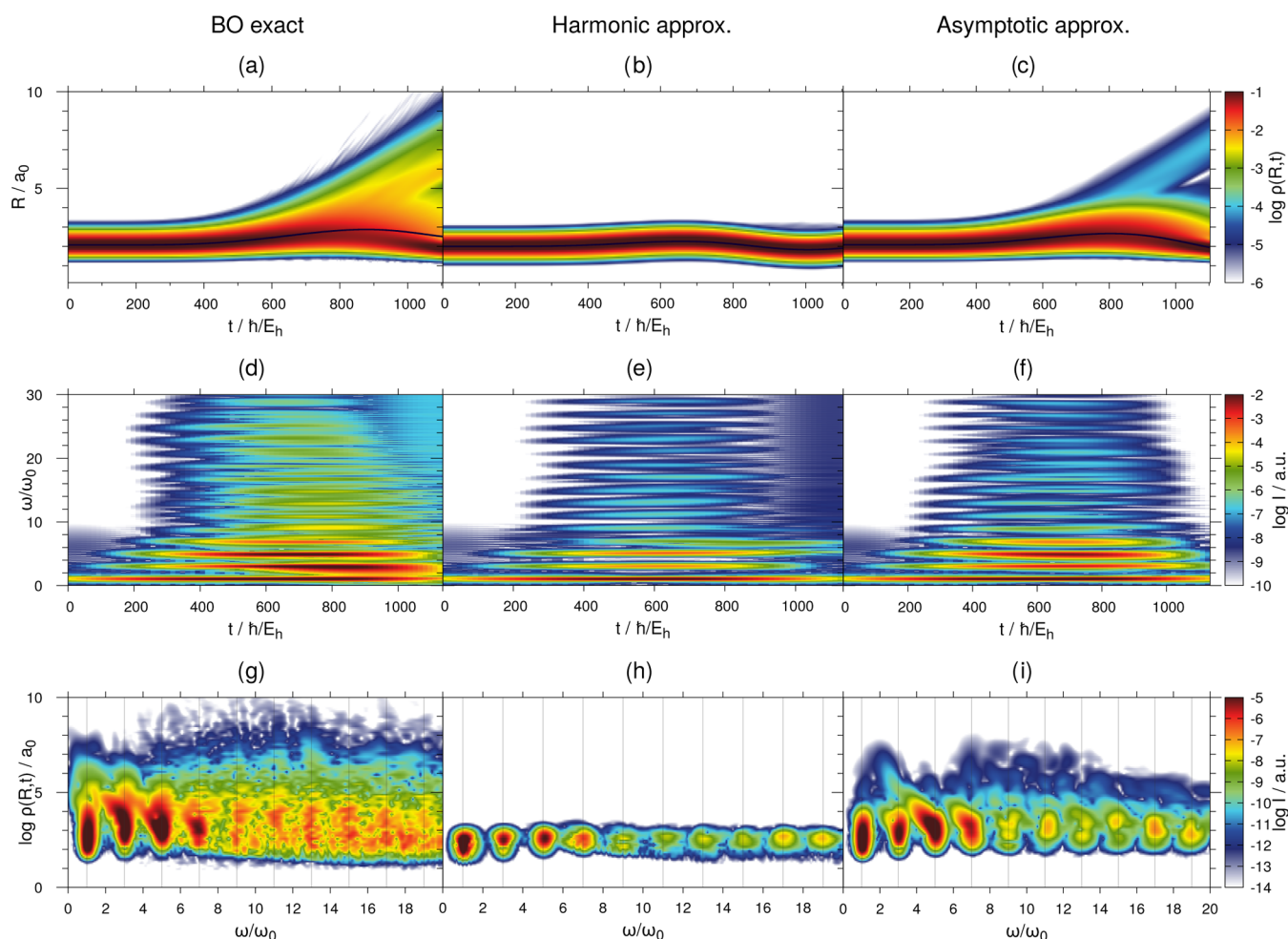


Figure 4. Deeper analysis of HHG spectra and related properties for the $E_0 = 0.09 \frac{E_h}{ea_0}$, 800 nm, 10-cycle pulse. Top (a–c): nuclear density $\rho(R,t)$ with distance expectation value $\langle R \rangle(t)$ (black line) indicated; middle row (d–f): time-dependent HHG spectra, $I(t;\omega)$; bottom (g–i): R -dependent HHG spectra, $I(R;\omega)$; left (a, d, g): “exact BO” solution; middle column (b, e, h): “harmonic approximation”; and right (c, f, i): “asymptotic approximation”.

approximation. In fact, using the harmonic approximation for all states except for the first excited state, and using for that one its exact potential curve $V(R)$, removes this resonance feature (not shown). Further, smaller differences between harmonically and asymptotically approximated schemes are seen for the lowest few harmonics at higher field intensities (Figure 2b, with inset, and (c)). This indicates that the harmonic

approximation needs to be applied with special care if dissociative potential energy surfaces are important for the HHG process.

We also disentangled the potential and dipole approximations used in this work. HHG spectra obtained with “exact potentials” but the “exact dipoles” replaced by Herzberg-Teller ones, gave very similar results to “exact potentials” with

“exact dipoles” (not shown). Other properties can be more affected when using the HT approximation. This is demonstrated for the bondlength expectation value $\langle R \rangle(t) = \langle \Psi(\underline{r}, R; t) | R | \Psi(t) \rangle_{\underline{r}, R; L^2}$, obtained from the total wavefunction, and for the dipole moment along the molecular axis, $\mu_z(t)$ (see Section 2.3), as shown in Figure 3a,b, respectively. Note that dipole moments obtained with “exact potentials” and “exact dipoles” (“BO exact”) are very similar to those obtained with “exact potentials” and HT dipoles (“BO + HT dipoles”), except at long times (Figure 3b). The additional harmonic and asymptotic potential approximations have a bigger effect on $\mu_z(t)$, especially the former. Effects of both the potential and dipole approximations are somewhat larger for $\langle R \rangle(t)$ (Figure 3a).

In summary, while the agreement between approximated-potential/dipole and “exact BO” solutions is not perfect, the approximate schemes follow nicely the general trends predicted by “exact BO” and can therefore be considered as valuable, economic tools for predicting HHG spectra of more complicated molecules for which the computation of (many) potential energy surfaces is cumbersome or even impossible. Before considering such cases, a deeper analysis of the approximate BO schemes for H_2^+ is advisable.

4.1.2. In-Depth Analysis for H_2^+ . To analyze the influence of nuclear dynamics on spectra, three further quantities are used: First, the nuclear density $\rho(R; t) = \int |\Psi(\underline{r}, R; t)|^2 d\underline{r}$ is computed, showing the nuclear motion as a function of time. Second, a time-windowed Fourier transformation of the dipole moment is done according to eq 12, giving a time-resolved HHG spectrum $I(t; \omega)$, similar to what was presented in ref 7. Third, R -dependent HHG spectra $I(R; \omega)$ are computed according to eq 11. $R(t)$, $I(t; \omega)$, and $I(R; \omega)$ are shown, for a field amplitude of $E_0 = 0.09 \frac{E_h}{ea_0}$ in Figure 4, for “exact Born–Oppenheimer” and the two approximate methods, “harmonic” and “asymptotic” (the latter two with Herzberg–Teller dipoles). The corresponding Figure S1 for $E_0 = 0.03 \frac{E_h}{ea_0}$ is given in the Supporting Information.

The “exact BO” method shows a nuclear density evolution (Figure 4a) with a main strand around the equilibrium distance $R_0 = 1.98a_0$, following closely the expectation value $\langle R \rangle$ (black line, see also Figure 3), which starts oscillating with the laser pulse. At around $800 \frac{\hbar}{E_h}$, a second strand emerges, signifying the onset of partial dissociation. This behavior is reflected by the “asymptotic” (Figure 4c) but not by the “harmonic” approximation (Figure 4b), which does not allow for dissociation by definition.

The time-resolved HHG spectrum resulting from “exact BO” (Figure 4d) shows that fundamental harmonics are emitted throughout the laser pulse (starting at 0 and ending at $1103.2 \frac{\hbar}{E_h}$), with the lowest harmonics 1, 3, and 5 being chronologically/time-delayed emitted in this order, while in the plateau region, the emission of signals is more simultaneous. Apart from the overall lower HHG intensities (see above), a very similar behavior is found for both the “harmonic” and “asymptotic” approximations (Figure 4e,f), i.e., the profound differences in $\rho(R, t)$ between the two are largely washed out even in the t -resolved HHG spectra.

While time-resolved HHG spectra are experimentally known (see ref 62 and references therein), R -dependent HHG spectra are probably hard to measure. Yet they are useful for theoretical analysis.⁷ The R -dependent HHG spectrum for

“BO exact” (Figure 4g) reveals that harmonics are not predominantly emitted at equilibrium distance, $R_0 = 1.98a_0$, but when the molecule is stretched to about $3.5a_0$, i.e., outside the Franck–Condon region, as known from earlier literature.⁷ Here, a clear shift in the third and fifth harmonic to lower energies is visible at higher distance, coinciding with the observations of the t -resolved HHG spectrum that shows intensity at these energies at the end of the pulse, when the wavepacket has moved to larger distances. The R -dependent distribution of even higher harmonics is mostly scattered, showing maxima around uneven harmonic numbers and some at even. These shifts to lower energies also coincide with earlier theoretical observations of Silva et al., that link the suppression of odd and appearance of even harmonics to the appearance of a permanent dipole moment by electron localization in the dissociation of homonuclear molecules.⁷

Compared to these results, the nuclear density in the harmonic potential is restricted to smaller R -values around R_0 of $\sim 2a_0$. Therefore, also the R -dependent HHG spectrum (Figure 4h) is limited to positions around R_0 . This explains the lower intensity of HHG signals in the “harmonic approximation” compared to “exact BO”.

The large anharmonicity of the system is better accounted for in the “asymptotic approximation”. The corresponding R -dependent HHG spectrum agrees better with the “exact BO” one and allows for the emission of harmonics at larger R values in particular for harmonics 1, 3, 5, and 7. In fact, the HHG intensity difference between “approximate” and “exact BO” for these peaks is much lower for “asymptotic” than for the “harmonic” approximation according to Figure 2b. Further (intensity) differences between “exact BO” and “approximate” schemes for higher harmonics are found and can partially be traced back to the absent (“harmonic”) or reduced (“asymptotic”) onset of dissociation.

In passing, we note that a HHG and also R -dependent HHG spectrum for H_2^+ very close to the harmonic approximation can be obtained, when performing single-point (fixed- R) calculations at various R -values, R_p and then weighting with the ground-state nuclear density at these points, $\rho(R_p) = \int |\Psi(\underline{r}, R_p; t=0)|^2 d\underline{r}$ (not shown). This weighting procedure has been shown in ref 9 to already significantly improve the “fixed-nuclei” approach to HHG spectra when compared to more exact approaches that took anharmonic nuclear motion into account (cf. Figure 1 in ref 9). The weighted R approach is thus an alternative procedure for arriving at HHG spectra for vibrating molecules, of about the same accuracy as the “harmonic approximation” used in this work.

4.2. HHG Spectra of H_2 and LiH. The approximation schemes for potential curves (and dipole moments) were applied for the molecules hydrogen, H_2 , and lithium hydride, LiH, with two and four electrons, respectively. For these, the electronic potentials and dipole moments were constructed on configuration interaction singles (CIS) level in an active space involving the two valence electrons only in each case. Not the full anharmonic potentials but their harmonic and asymptotic approximations were calculated instead. Using the basis sets described in Section 3.2.2, we end up with 115 states for H_2 and 130 states for LiH. For the (transition) dipole moments, the Herzberg–Teller approximation was used. Further, H_2 was stimulated with an 800 nm, 10-cycle laser pulse with amplitude $E_0 = 0.09 \frac{E_h}{ea_0}$, and for LiH the same pulse with $E_0 = 0.03 \frac{E_h}{ea_0}$ was used. In addition to the “harmonic” and “asymptotic” (plus

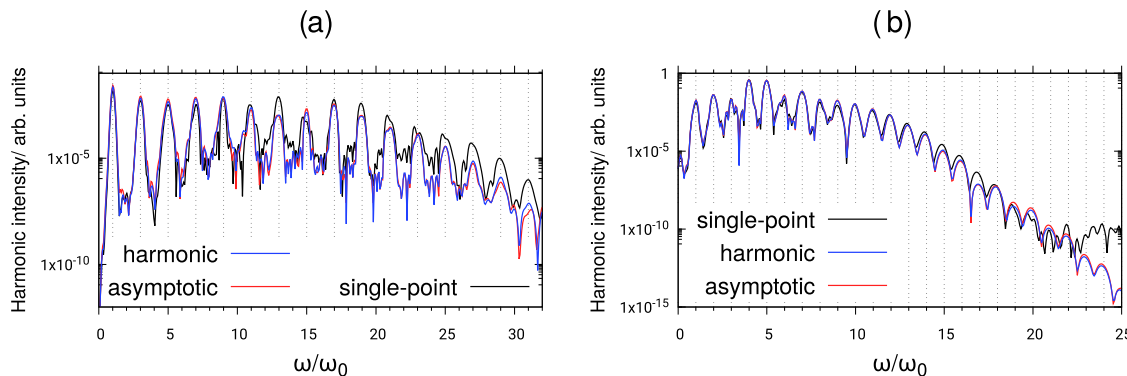


Figure 5. (a) HHG spectra (*y*-axis in arbitrary units, logarithmic scale) for H₂ resulting from an $E_0 = 0.09 \frac{E_h}{ea_0}$, 800 nm, 10-cycle laser pulse. (b) Same for LiH, using an $E_0 = 0.03 \frac{E_h}{ea_0}$, 800 nm, 10-cycle laser pulse. Spectra in single-point approximation in black, in harmonic approximation in blue, and in asymptotic approximation in red.

Herzberg–Teller) approximations, we also performed “single-point” (fixed-nuclei) calculations, with $R_0 = 1.388a_0$ and $R_0 = 3.038a_0$ for H₂ and LiH, respectively, as mentioned above. The HHG spectra resulting from all three approximations are shown in Figure 5.

For H₂, only odd harmonics are seen and the Born–Oppenheimer propagations on harmonic and asymptotic potential curves lead to different HHG intensities compared to the single-point calculations. Despite the differences for the lowest harmonics seem vanishingly small on the logarithmic scale, there are some, even for the fundamental. With increasing harmonics number, the differences between single-point and Born–Oppenheimer treatments get larger. The differences not only refer to HHG intensities but to lineshapes as well. Comparing the “harmonic” and “asymptotic” models to include nuclear motion shows that the agreement between the two is quite good for this molecule. Closer inspection shows that the intensities differ slightly.

For LiH, both even and odd harmonics are seen as expected. Here, differences of the two models with nuclear motion to the single-point method are smaller than for H₂, both with a shape and intensity of HHG signals. This has to do with the higher (reduced) mass in combination pulse that is short compared to the nuclear vibrational period. Still, some quantitative differences occur, even for the intensity of the fundamental, but more so for harmonics beyond about the 15th. (For the higher harmonics, nonlinear contributions to the dipoles, not included in the Herzberg–Teller approximation, become more severe.) Note also that for LiH, the agreement between “harmonic” and “asymptotic” approximations is very good. The good agreement between both approximated methods for these many-electron systems reflects their higher harmonicity compared to H₂⁺.

4.3. HHG Spectra of a Polyatomic Molecule: H₂O. Further, we computed HHG spectra for the water molecule to demonstrate the applicability of the mentioned approximations for polyatomic molecules with more than one nuclear coordinate. In particular, we apply the “harmonic” potential approximation in combination with the Condon approximation for dipole moments. Here, just the harmonic approximation is used as the most promising route to polyatomic systems. It reduces the necessary grid size and it is reasonable because for H₂O, less dissociative behavior is expected than for H₂ or LiH. In the spirit of the approximate methods to treat the spectroscopy mentioned in the Section 1, e.g., the

independent mode displaced harmonic oscillator models, one would work with $3M - 6$ normal modes and coordinates of an *M*-atomic, nonlinear molecule, obtained from normal mode analysis. By decoupling the modes, the solution of the nuclear Schrödinger equation and thus of (HHG) spectra would be greatly simplified. In the case of H₂O, the normal mode analysis gives the usual high-frequency symmetric stretch and asymmetric stretch modes, and the low-frequency bending mode.

Here, in this proof-of-principle paper, we follow a slightly different route. First of all, we neglect the low-frequency bending mode. Second, at a fixed H–O–H bond angle, we Taylor-expand up to second order, i.e., harmonically, the potential around the minimum (R_0^x, R_0^y), where R_0^x and R_0^y are the corresponding two O–H bondlengths in the electronic ground state. Thus

$$\begin{aligned} V(x, y) = & V(R_0^x, R_0^y) + V'_x \cdot (x - R_0^x) + \frac{1}{2} V''_{xx} \\ & \cdot (x - R_0^x)^2 + V'_y \cdot (y - R_0^y) + \frac{1}{2} V''_{yy} \\ & \cdot (y - R_0^y)^2 + V''_{xy} \cdot (x - R_0^x)(y - R_0^y) \end{aligned} \quad (17)$$

with

$$\begin{aligned} V''_{xy} = & \frac{1}{4\Delta x \Delta y} (V(R_0^x + \Delta x, R_0^y + \Delta y) \\ & - V(R_0^x + \Delta x, R_0^y - \Delta y) \\ & - V(R_0^x - \Delta x, R_0^y + \Delta y) \\ & + V(R_0^x - \Delta x, R_0^y - \Delta y)) \end{aligned} \quad (18)$$

In these equations, *x* and *y* are coordinates along the two bonds, V' and V'' are first and second derivatives, along *x* and *y*, at R_0^x and R_0^y . Δx and Δy are step sizes to obtain the derivatives, chosen here as $\Delta x = \Delta y = 0.1a_0$. This expansion is used for every electronic state *j* as before, giving potential energy surfaces $V_j(x, y)$. Note that, for the ground state, *j* = 0, first derivatives are zero, while for higher states, *j* > 0, they are not and $V_j(R_0^x, R_0^y)$ is the vertical Franck–Condon excitation energy from the ground state to state *j*, when we set $V_0(R_0^x, R_0^y) = 0$. We do not work with decoupled (constrained) normal modes here but directly solve the two-dimensional, coupled nuclear TDSEs of the type (8) numerically instead. There,

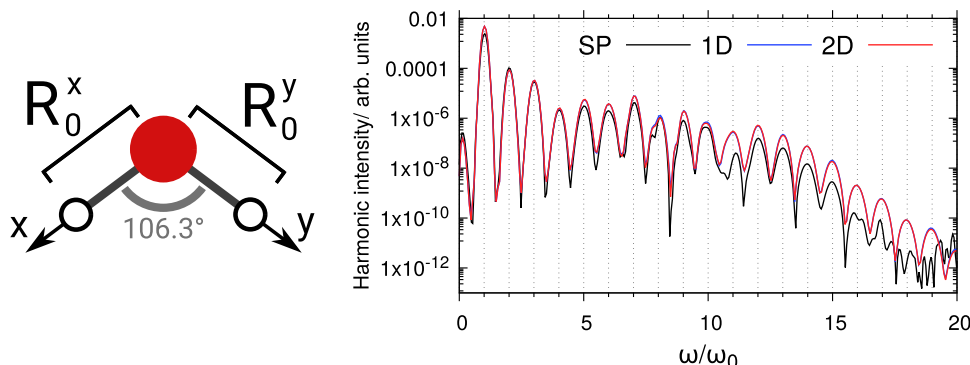


Figure 6. Left: Water molecule and the used 2D coordinate system with equilibrium distances indicated. Right: HHG spectra of a H_2O molecule, stimulated with a 10-cycle, 800 nm laser pulse with $E_0 = 0.04 \frac{E_h}{ea_0}$ polarized in the direction of the molecular symmetry axis (i.e., along its permanent dipole moment). “SP” denotes a single-point (fixed-nuclei) calculation, while in “1D” and “2D” one or two nuclear coordinates are included in the Born–Oppenheimer approximation with harmonically approximated potentials and under the Condon approximation. The 1D solution is almost exactly coinciding with the 2D one.

nuclear Hamiltonian matrix elements being $\hat{H}_{ij}(t) = \left(-\frac{1}{2m} \frac{\partial^2}{\partial x^2} - \frac{1}{2m} \frac{\partial^2}{\partial y^2} + V_i(x, y) \right) \delta_{ij} - \underline{\mu}_{ij} \underline{E}(t)$ and m taken as the reduced mass of an O–H bond, $m = m_{\text{H}} m_{\text{O}} / (m_{\text{H}} + m_{\text{O}}) = 1728.26 \text{ } m_e$.

Technically, the O–H potentials were expanded around the minimum O–H bondlength $R_0^x = R_0^y = 1.778a_0$ (0.941 Å), obtained from a restricted Hartree–Fock calculation using the aug-cc-pVTZ basis set, at an optimized, fixed H–O–H bond angle of 106.3°. For the nuclear wavepacket propagation, a two-dimensional grid with 64 points between [0.15a₀, 3.35a₀] in each O–H coordinate was adopted. A Runge–Kutta fourth-order propagator with a time step of 0.02 \hbar/E_h was used, starting from the ground state of the adiabatic potential, obtained from diagonalizing a Fourier-Grid-Hamiltonian.⁶³ Electronically excited states were determined as before, using the aug-cc-pVTZ basis set with the first eight Kaufmann shells centered around the molecular center of mass, on the CIS level of theory based on Hartree–Fock orbitals, adapted from Psi4. This resulted in 637 CIS state functions, when the 1s electrons of oxygen were frozen.

As said, permanent and transition dipole moments were treated as constants (Condon approximation).

The H_2O molecule was stimulated by a 10-cycle, 800 nm laser pulse of \cos^2 shape with $E_0 = 0.04 \frac{E_h}{ea_0}$. Different polarization directions were chosen. Here, we show only the results for polarization along the molecule’s symmetry axis, which should couple the most to nuclear motion and has the highest polarizabilities. The HHG spectra are evaluated in the direction of laser polarization.

In addition to the 2D propagation, we also computed HHG spectra in the fixed-nuclei approximation (SP), and also using a 1D model in which only one O–H bond was allowed to move. (For another fixed-nuclei calculation for the HHG spectrum of H_2O , see ref 64, which however uses rather different pulse parameters.) The corresponding HHG spectra are shown in Figure 6.

From the figure, we first of all note even and odd harmonics and a plateau region sandwiched between a high-intensity, low-harmonic and a low-intensity, high-harmonic region. When comparing the fixed-nuclei/single-point (SP) calculation to those where nuclear motion was allowed for, we see that the SP spectrum differs from the other two. The SP solution

predicts lower HHG intensities and shows some artificial, nonsmooth structures. Again, deviations are stronger when the harmonics are higher. Interestingly, the 1D and 2D HHG spectra almost coincide. This becomes much more clear in a normal mode picture. Here, only the symmetric stretch can have displaced minima in the excited-state potential energy surfaces, while the asymmetric stretch minima are fixed at $R_0^x = R_0^y$ due to symmetry. Hence, only the symmetric stretch couples strongly to the nuclear motion, reducing it almost to a one-dimensional problem. Seemingly, the 1D propagation already covers most of this behavior with a second mode only slightly complementing it.

5. CONCLUSIONS

In this work, laser-driven coupled nuclear-electron dynamics, leading to high harmonic generation (HHG), was modeled by Born–Oppenheimer dynamics adopting a multistate expansion, using Gaussian-orbital based methods for the electronic structure part. Both nuclei and electrons are treated quantum mechanically. The method gives, for H_2^+ , HHG spectra close to an “all-grid” solution.⁹ Replacing the “exact” potential curves for H_2^+ by “harmonically” or “asymptotically” approximated ones, and the “exact” (transition) dipole moments by constant-dipole (Condon approximation) or linear dipole functions (Herzberg–Teller approximation), constitutes a set of approximate methods that require comparatively little input from ab initio calculations, similar in spirit to approximations like the displaced harmonic oscillator models known from molecular, vibronic spectroscopy.

It is found that these approximate methods qualitatively, sometimes semiquantitatively, reproduce HHG spectra obtained from “exact Born–Oppenheimer” dynamics. They also go clearly beyond the fixed-nuclei approximation and explain details of effects of nuclear dynamics on the electronic response. This was not only shown for H_2^+ but also for molecules with more than one electron as the diatomic H_2 and LiH and a polyatomic molecule, H_2O , for which the underlying electronic structure problems were solved by a configuration interaction singles (CIS) scheme. The latter, in concert with a simple heuristic ionization model and together with the additional approximations made here, establishes an efficient route toward the quantum mechanical modeling of ultrafast, coupled nuclear dynamics of laser-driven, complex molecules.

The methods should be applicable to attochemical problems beyond HHG.

Appendix

A. Harmonic Approximation. Considering an electronic potential for a diatomic molecule, $V(R)$, a quadratic potential $V^{\text{HO}}(R) \approx V(R)$ can be obtained from a Taylor expansion to second order, at point R_0 , as

$$\begin{aligned} V^{\text{HO}}(R) &= V + \frac{dV(R)}{dR} \Big|_{R_0} (R - R_0) + \frac{1}{2} \frac{d^2V(R)}{dR^2} \Big|_{R_0} (R - R_0)^2 \\ &= V + V'(R - R_0) + \frac{1}{2} V''(R - R_0)^2 \\ &= A(R - R_{\min})^2 + E_{\min} \end{aligned} \quad (19)$$

V , V' , and V'' correspond here to the values at R_0 of the electronic potential and its first and second derivatives. To arrive at the last factorized form, first, the parameter A is determined from the comparison of coefficient with R^2 : $A = \frac{1}{2}V''$. The potential minimum parameter, R_{\min} , can be calculated from the first derivative with respect to R

$$0 = V' + V''(R_{\min} - R_0) \Leftrightarrow R_{\min} = R_0 - \frac{V'}{V''} \quad (20)$$

Inserting $R_{\min} - R_0 = -\frac{V'}{V''}$ into the potential gives the minimum energy, E_{\min}

$$\begin{aligned} V^{\text{HO}}(R_{\min}) &= E_{\min} = V + V'\left(-\frac{V'}{V''}\right) + \frac{1}{2}V''\left(-\frac{V'}{V''}\right)^2 \\ &\Leftrightarrow E_{\min} = V - \frac{V'^2}{2V''} \end{aligned} \quad (21)$$

as stated in the main text. For a propagation with these potentials, two computational adaptions were taken into account: First, an energetic cutoff was set at $+5E_h$ above E_{\min} , as well as at $-1E_h$ below the exact energy, V , or, if higher, at $E_{\min,0}$ of the ground state, for each electronic state separately. Second, potentials with a negative curvature, $A < 0$, were created with positive curvature instead, $A^* = |A|$, therefore, also changing the position of their minimum. The justification for that harsh alteration of the potential is a great improvement in computational stability of the potentials. Additionally, these negative curvatures (at least in small molecules as H_2^+) appear, most likely, only because of avoided crossings, having little systematic impact on the dynamics.

B. Derivative Step ΔR . The derivatives of the potential are calculated from three points $V(R_0 - \Delta R)$, $V(R_0)$, and $V(R_0 + \Delta R)$

$$V' = \frac{V(R_0 + \Delta R) - V(R_0 - \Delta R)}{2\Delta R} + O(\Delta R^2) \quad (22)$$

$$\begin{aligned} V'' &= \frac{V(R_0 + \Delta R) - 2V(R_0) + V(R_0 - \Delta R)}{\Delta R^2} \\ &\quad + O(\Delta R^2) \end{aligned} \quad (23)$$

The step size ΔR showed good, stable results for $10^{-1}a_0 \geq \Delta R > 10^{-3}a_0$. Smaller step sizes decrease the effect of possible conical intersections and avoided crossings and their impact on

the accuracy of derivatives. On the other hand, too small derivative steps also introduce errors based on the limited numerical precision of the underlying electronic calculations. Therefore, a step size of $10^{-3}a_0$ was chosen. This is, for H_2^+ , the smallest value agreeing in the ground-state curvature, A_0 , with the longer steps of $0.01a_0$ and $0.1a_0$, which should describe the harmonic fit reasonably well (see Table 1).

Table 1. Harmonic Approximation Parameters for the Ground State of H_2^+ , Calculated with Different Derivative Steps ΔR at $R_0 = 1.98a_0$

$\Delta R [a_0]$	A_0	$R_{\min,0} [a_0]$
1.0×10^{-8}	1.93×10^6	1.98
1.0×10^{-6}	128.506	1.98001
1.0×10^{-5}	8.27006	1.98011
1.0×10^{-4}	0.124414	1.98776
0.001	0.0535355	1.99805
0.01	0.0538546	1.99799
0.1	0.0541252	2.00207

C. Asymptotic Approximation. With the first two derivatives of the electronic potential at R_0 , V , V' , and V'' , an asymptotic approximation can be constructed by expanding it in reciprocal factors of $\frac{1}{R}$ ^{59,60}

$$V^{\text{asym}}(R) = B_0 + B_1 \frac{1}{R} + B_2 \left(\frac{1}{R}\right)^2 \quad (24)$$

To obtain coefficients, three simultaneous equations have to be solved

$$\begin{cases} \text{I } V &= B_0 + B_1 \frac{1}{R} + B_2 \left(\frac{1}{R}\right)^2 \\ \text{II } V' &= -B_1 \left(\frac{1}{R}\right)^2 - 2B_2 \left(\frac{1}{R}\right)^3 \\ \text{III } V'' &= 2B_1 \left(\frac{1}{R}\right)^3 + 6B_2 \left(\frac{1}{R}\right)^4 \end{cases} \quad (25)$$

These equations are investigated at $R = R_0$. Multiplying each with R_0^n , with n being the highest exponent of $\frac{1}{R}$, yields

$$\begin{cases} \text{I } VR_0^2 &= B_0 R_0^2 + B_1 R_0 + B_2 \\ \text{II } V'R_0^3 &= -B_1 R_0 - 2B_2 \\ \text{III } V''R_0^4 &= 2B_1 R_0 + 6B_2 \end{cases} \quad (26)$$

From $2 \cdot \text{II} + \text{III}$, B_2 can be calculated

$$2V'R_0^3 + V''R_0^4 = 0 + 2B_2 \Leftrightarrow B_2 = V'R_0^3 + \frac{1}{2}V''R_0^4 \quad (27)$$

From II follows an expression for B_1

$$\begin{aligned} V'R_0^3 &= -B_1 R_0 - 2B_2 \Leftrightarrow B_1 = -\left(V'R_0^2 + \frac{2B_2}{R_0}\right) \\ &= -(3V'R_0^2 + V''R_0^3) \end{aligned} \quad (28)$$

B_0 can be determined from I

$$\begin{aligned} V &= B_0 + B_1 \frac{1}{R} + B_2 \left(\frac{1}{R} \right)^2 \Leftrightarrow B_0 = V - \frac{B_1}{R_0} - \frac{B_2}{R_0^2} \\ &= V + 2 V' R_0 + \frac{1}{2} V'' \end{aligned} \quad (29)$$

The potential creates a function with a possible minimum at (R_{\min}, E_{\min}) with a scaling of C

$$\begin{aligned} V^{\text{asym}}(R) &= B_0 + B_1 \frac{1}{R} + B_2 \left(\frac{1}{R} \right)^2 \\ &= E_{\min} + C \left(\frac{1}{R} - \frac{1}{R_{\min}} \right)^2 \end{aligned} \quad (30)$$

Equating coefficients gives three equations

$$\begin{cases} \text{I} \quad B_0 = E_{\min} - C \left(\frac{1}{R_{\min}} \right)^2 \\ \text{II} \quad B_1 = -2 C \frac{1}{R_{\min}} \\ \text{III} \quad B_2 = C \end{cases} \quad (31)$$

Inserting III into II, yields

$$B_1 = -2 B_2 \frac{1}{R_{\min}} \Leftrightarrow R_{\min} = -2 \frac{B_2}{B_1} \quad (32)$$

The minimum energy results then from I

$$B_0 = E_{\min} - B_2 \left(\frac{1}{-2 \frac{B_2}{B_1}} \right)^2 \Leftrightarrow E_{\min} = B_0 - \frac{B_1^2}{4 B_2} \quad (33)$$

Additionally, the curvature at R_{\min} , a , can be determined as a second derivative

$$\begin{aligned} a &= V''(R_{\min}) = 2 B_1 \left(\frac{1}{R_{\min}} \right)^3 + 6 B_2 \left(\frac{1}{R_{\min}} \right)^4 \\ &= 2 B_1 \left(\frac{1}{R_{\min}} \right)^3 + 6 B_2 \left(\frac{1}{R_{\min}} \right)^3 \left(-\frac{B_1}{2 B_2} \right) \\ &= -\frac{B_1}{R_{\min}^3} \end{aligned} \quad (34)$$

The advantage of this representation is the modeling of unbound and bound states with a dissociative energy of $B_0 - E_{\min}$. For computational reasons, a cutoff was introduced at $+S E_h$ above the dissociative limit B_0 . Also, for potentials with maxima instead of minima (negative curvature, $a < 0$) and $R_{\min} > 0$, were set to $V(R) = E_{\min}$ for smaller distances $R < R_{\min}$.

An additional problem arises if the dissociative limit, equal to $B_{0,j}$ of a potential j becomes lower than that of the lower lying states, $B_{0,j} < B_{0,j-1}$, or even the ground state, $B_{0,j} < B_{0,0}$, enabling computational errors and instability. In these cases, the asymptotic fit was developed differently, with matching V and V' and a user-specified dissociative limit in the form of the coefficient $B_{0,j}^*$, e.g., that of the lower lying state, $B_{0,j-1}$. This is done under the assumption that adiabatic states, without crossings, will asymptotically reach at most to the dissociation

limit of the lower lying state:
 $B_{0,j} = \lim_{R \rightarrow \infty} V_j(R) \geq \lim_{R \rightarrow \infty} V_{j-1}(R) = B_{0,j-1}$.

The new coefficients can be derived from the three conditions of first, the changed dissociation limit, $B_0^* = B_{0,j-1}$, second, the intersection in R_0 , $V^{\text{asym}}(R_0) = V$, and third, the shared inclination in R_0

$$\begin{cases} \text{I} \quad B_0^* = B_{0,j-1} \\ \text{II} \quad V = B_0^* + B_1^* \left(\frac{1}{R_0} \right) + B_2^* \left(\frac{1}{R_0} \right)^2 \\ \text{III} \quad V' = -B_1^* \left(\frac{1}{R_0} \right)^2 - 2 B_2^* \left(\frac{1}{R_0} \right)^3 \end{cases} \quad (35)$$

$2 \cdot \text{II} + \text{III} \cdot R_0$ yield B_1^*

$$\begin{aligned} 2 V + V' R_0 &= 2 B_0^* + 2 B_1^* \frac{1}{R_0} - B_1^* \frac{1}{R_0} + 0 \Leftrightarrow B_1^* \\ &= (2 V + V' R_0 - 2 B_0^*) R_0 \end{aligned} \quad (36)$$

and $\text{II} + \text{III} \cdot R_0$ yield B_2^*

$$\begin{aligned} V + V' R_0 &= B_0^* + 0 + B_2^* \left(\frac{1}{R_0} \right)^2 - 2 B_2^* \left(\frac{1}{R_0} \right)^2 \Leftrightarrow B_2^* \\ &= -(V + V' R_0 - B_0^*) R_0^2 \end{aligned} \quad (37)$$

This alternative calculation leaves a small disadvantage in possibly introducing new minima in beforehand unbound states, especially for steep inclinations.

ASSOCIATED CONTENT

Supporting Information

The Supporting Information is available free of charge at <https://pubs.acs.org/doi/10.1021/acs.jpca.3c01811>.

Deeper analysis of dynamic properties of BO and approximated propagations for $E_0 = 0.03 \frac{E_h}{ea_0}$ and HHG spectra for approximations using a reference point $R_0 = 1.9994 a_0$ ([PDF](#))

AUTHOR INFORMATION

Corresponding Author

Paul Anton Albrecht – Universität Potsdam, Institut für Chemie, D-14476 Potsdam-Golm, Germany; [orcid.org/0000-0001-8829-3298](#); Email: paul.albrecht@uni-potsdam.de

Authors

Christoph Witzorky – Universität Potsdam, Institut für Chemie, D-14476 Potsdam-Golm, Germany

Peter Saalfrank – Universität Potsdam, Institut für Chemie, D-14476 Potsdam-Golm, Germany; Universität Potsdam, Institut für Physik und Astronomie, D-14476 Potsdam-Golm, Germany; [orcid.org/0000-0002-5988-5945](#)

Tillmann Klamroth – Universität Potsdam, Institut für Chemie, D-14476 Potsdam-Golm, Germany; [orcid.org/0000-0001-5555-5490](#)

Complete contact information is available at:

<https://pubs.acs.org/10.1021/acs.jpca.3c01811>

Notes

The authors declare no competing financial interest.

ACKNOWLEDGMENTS

Financial support by the Deutsche Forschungsgemeinschaft (DFG) through Project Grant Sa 547/14-1 and Kl 1387/5-1 is gracefully acknowledged. P.A.A. acknowledges support by the IMPRS for Elementary Processes in Physical Chemistry.

REFERENCES

- (1) Midorikawa, K. High-Order Harmonic Generation and Attosecond Science. *Jpn. J. Appl. Phys.* **2011**, *50*, No. 090001.
- (2) Corkum, P. B.; Krausz, F. Attosecond Science. *Nat. Phys.* **2007**, *3*, 381–387.
- (3) Gaumnitz, T.; Jain, A.; Pertot, Y.; Huppert, M.; Jordan, I.; Ardanza-Lamas, F.; Wörner, H. Streaking of 43-attosecond soft-X-ray pulses generated by passively CEP-stable mid-infrared driver. *Opt. Express* **2017**, *25*, 27506–27518.
- (4) Schmidt, C.; Pertot, Y.; Belciunas, T.; Zinchenko, K.; Mathews, M.; Wörner, H. J.; Wolf, J.-P. High-order harmonic source spanning up to the oxygen K-edge based on filamentation pulse compression. *Opt. Express* **2018**, *26*, 11834–11842.
- (5) Corkum, P. B. Plasma perspective on strong field multiphoton ionization. *Phys. Rev. Lett.* **1993**, *71*, 1994–1997.
- (6) Chirilă, C. C.; Lein, M. Influence of nuclear vibration on harmonic generation in molecules. *J. Phys. B: At., Mol. Opt. Phys.* **2006**, *39*, S437–S444.
- (7) Silva, R. E. F.; Rivière, P.; Morales, F.; Smirnova, O.; Ivanov, M.; Martín, F. Even harmonic generation in isotropic media of dissociating homonuclear molecules. *Sci. Rep.* **2016**, *6*, No. 32653.
- (8) Labeye, M.; Zapata, F.; Coccia, E.; Vénard, V.; Toulouse, J.; Caillat, J.; Taieb, R.; Luppi, E. *J. Chem. Theor. Comput.* **2018**; Vol. 14, p 5846.
- (9) Witzorky, C.; Paramonov, G.; Bouakline, F.; Jaquet, R.; Saalfrank, P.; Klamroth, T. Gaussian-Type Orbital Calculations for High Harmonic Generation in Vibrating Molecules: Benchmarks for H₂⁺. *J. Chem. Theory Comput.* **2021**, *17*, 7353–7365. PMID: 34747605.
- (10) Paramonov, G. K.; Klamroth, T.; Lu, H. Z.; Bandrauk, A. D. Quantum dynamics, isotope effects, and power spectra of H₂⁺ and HD⁺ excited to the continuum by strong one-cycle laser pulses: Three-dimensional non-Born-Oppenheimer simulations. *Phys. Rev. A* **2018**, *98*, No. 063431.
- (11) Paramonov, G. K.; Saalfrank, P. Muonic molecular ions *ppμ* and *pdu* driven by superintense VUV laser pulses: Postexcitation muonic and nuclear oscillations and high-order harmonic generation. *Phys. Rev. A* **2018**, *97*, No. 053408.
- (12) Kanai, T.; Minemoto, S.; Sakai, H. Quantum interference during high-order harmonic generation from aligned molecules. *Nature* **2005**, *435*, 470–474.
- (13) McFarland, B. K.; Farrell, J. P.; Bucksbaum, P. H.; Gühr, M. High Harmonic Generation from Multiple Orbitals in N₂. *Science* **2008**, *322*, 1232–1235.
- (14) Rupenyan, A.; Kraus, P. M.; Schneider, J.; Wörner, H. J. Quantum interference and multielectron effects in high-harmonic spectra of polar molecules. *Phys. Rev. A* **2013**, *87*, No. 031401.
- (15) Wong, M. C. H.; Brichta, J.-P.; Spanner, M.; Patchkovskii, S.; Bhardwaj, V. R. High-harmonic spectroscopy of molecular isomers. *Phys. Rev. A* **2011**, *84*, No. 051403.
- (16) Hutchison, C.; Ganeev, R. A.; Castillejo, M.; Lopez-Quintas, I.; Zaïr, A.; Weber, S. J.; McGrath, F.; Abdelrahman, Z.; Oppermann, M.; Martin, M.; et al. Comparison of high-order harmonic generation in uracil and thymine ablation plumes. *Phys. Chem. Chem. Phys.* **2013**, *15*, 12308–12313.
- (17) Marangos, J. P. Development of high harmonic generation spectroscopy of organic molecules and biomolecules. *J. Phys. B: At., Mol. Opt. Phys.* **2016**, *49*, No. 132001.
- (18) Bedurke, F.; Klamroth, T.; Krause, P.; Saalfrank, P. Discriminating organic isomers by high harmonic generation: A time-dependent configuration interaction singles study. *Chem. Phys.* **2019**, *150*, No. 234114.
- (19) Luppi, E.; Coccia, E. Probing the molecular frame of uracil and thymine with high-harmonic generation spectroscopy. *Phys. Chem. Chem. Phys.* **2021**, *23*, 3729–3738.
- (20) Zhou, S.; Li, Q.; Guo, F.; Wang, J.; Chen, J.; Yang, Y. High-order harmonic generation of benzene molecules irradiated by circularly polarized laser pulses. *Chem. Phys.* **2021**, *545*, No. 111147.
- (21) Avetissian, H. K.; Ghazaryan, A. G.; Mkrtchian, G. F. High harmonic generation in fullerene molecules. *Phys. Rev. B* **2021**, *104*, No. 125436.
- (22) Morassut, C.; Luppi, E.; Coccia, E. A TD-CIS study of high-harmonic generation of uracil cation fragments. *Chem. Phys.* **2022**, *559*, No. 111515.
- (23) Neufeld, O.; Wengrowicz, O.; Peleg, O.; Rubio, A.; Cohen, O. Detecting multiple chiral centers in chiral molecules with high harmonic generation. *Opt. Express* **2022**, *30*, 3729–3740.
- (24) Isborn, C. M.; Li, X. Singlet-Triplet Transitions in Real-Time Time-Dependent Hartree-Fock/Density Functional Theory. *J. Chem. Theory Comput.* **2009**, *5*, 2415–2419.
- (25) Chapman, C. T.; Liang, W.; Li, X. Ultrafast Coherent Electron-Hole Separation Dynamics in a Fullerene Derivative. *J. Phys. Chem. Lett.* **2011**, *2*, 1189–1192. PMID: 26295324.
- (26) Bedurke, F.; Klamroth, T.; Saalfrank, P. Many-electron dynamics in laser-driven molecules: wavefunction theory vs. density functional theory. *Phys. Chem. Chem. Phys.* **2021**, *23*, 13544–13560.
- (27) Deumens, E.; Öhrn, Y. Complete Electron Nuclear Dynamics. *Phys. Chem. A* **2001**, *105*, 2660–2667.
- (28) Nest, M. The multi-configuration electron-nuclear dynamics method. *Chem. Phys. Lett.* **2009**, *472*, 171–174.
- (29) Haxton, D. J.; Lawler, K. V.; McCurdy, C. W. Multi-configuration time-dependent Hartree-Fock treatment of electronic and nuclear dynamics in diatomic molecules. *Phys. Rev. A* **2011**, *83*, No. 063416.
- (30) Ulusoy, I. S.; Nest, M. The multi-configuration electron-nuclear dynamics method applied to LiH. *Chem. Phys.* **2012**, *136*, No. 054112.
- (31) Aebersold, L. E.; Ulusoy, I. S.; Wilson, A. K. Coupled electron and nuclear motion in strong laser fields. *Phys. Rev. A* **2019**, *100*, No. 023406.
- (32) Sirjoosinh, A.; Pak, M. V.; Brorsen, K. R.; Hammes-Schiffer, S. Quantum treatment of protons with the reduced explicitly correlated Hartree-Fock approach. *Chem. Phys.* **2015**, *142*, No. 214107.
- (33) Hammes-Schiffer, S. Nuclear–electronic orbital methods: Foundations and prospects. *Chem. Phys.* **2021**, *155*, No. 030901.
- (34) Chakraborty, A.; Pak, M. V.; Hammes-Schiffer, S. Properties of the exact universal functional in multicomponent density functional theory. *Chem. Phys.* **2009**, *131*, No. 124115.
- (35) Bandrauk, A. D.; Chelkowski, S.; Lu, H. Signatures of nuclear motion in molecular high-order harmonics and in the generation of attosecond pulse trains by ultrashort intense laser pulses. *J. Phys. B: At., Mol. Opt.* **2009**, *42*, No. 075602.
- (36) Anzaki, R.; Sato, T.; Ishikawa, K. L. A fully general time-dependent multiconfiguration self-consistent-field method for the electron–nuclear dynamics. *Phys. Chem. Chem. Phys.* **2017**, *19*, 22008–22015.
- (37) Li, Y.; Sato, T.; Ishikawa, K. L. Implementation of a time-dependent multiconfiguration self-consistent-field method for coupled electron-nuclear dynamics in diatomic molecules driven by intense laser pulses. *Phys. Rev. A* **2021**, *104*, No. 043104.
- (38) Krause, P.; Klamroth, T.; Saalfrank, P. Time-dependent configuration-interaction calculations of laser-pulse-driven many-electron dynamics: Controlled dipole switching in lithium cyanide. *Chem. Phys.* **2005**, *123*, No. 074105.
- (39) Rohringer, N.; Gordon, A.; Santra, R. Configuration-interaction-based time-dependent orbital approach for *ab initio*

- treatment of electronic dynamics in a strong optical laser field. *Phys. Rev. A* **2006**, *74*, No. 043420.
- (40) Schlegel, H. B.; Smith, S. M.; Li, X. Electronic optical response of molecules in intense fields: Comparison of TD-HF, TD-CIS, and TD-CIS(D) approaches. *J. Chem. Phys.* **2007**, *126*, No. 244110.
- (41) Luppi, E.; Head-Gordon, M. The role of Rydberg and continuum levels in computing high harmonic generation spectra of the hydrogen atom using time-dependent configuration interaction. *J. Chem. Phys.* **2013**, *139*, No. 164121.
- (42) Krause, P.; Sonk, J. A.; Schlegel, H. Strong field ionization rates simulated with time-dependent configuration interaction and an absorbing potential. *J. Chem. Phys.* **2014**, *140*, No. 174113.
- (43) Kato, T.; Kono, H. Time-dependent multiconfiguration theory for electronic dynamics of molecules in an intense laser field. *Chem. Phys. Lett.* **2004**, *392*, 533–540.
- (44) Zanghellini, F.; Kitzler, M.; Fabian, C.; Brabec, T.; Scrinzi, A. An MCTDHF approach to multi-electron dynamics in laser fields. *Laser Phys.* **2003**, *13*, 1064–1068.
- (45) Hochstuhl, D.; Bonitz, M. Two-photon ionization of helium studied with the multiconfigurational time-dependent Hartree–Fock method. *J. Chem. Phys.* **2011**, *134*, No. 084106.
- (46) Nest, M.; Klamroth, T.; Saalfrank, P. The multiconfiguration time-dependent Hartree–Fock method for quantum chemical calculations. *J. Chem. Phys.* **2005**, *122*, No. 124102.
- (47) Kvaal, S. Ab initio quantum dynamics using coupled-cluster. *J. Chem. Phys.* **2012**, *136* DOI: [10.1063/1.4718427](https://doi.org/10.1063/1.4718427).
- (48) Huber, C.; Klamroth, T. Explicitly time-dependent coupled cluster singles doubles calculations of laser-driven many-electron dynamics. *J. Chem. Phys.* **2011**, *134*, No. 054113.
- (49) Cederbaum, L. S.; Köppel, H.; Domcke, W. Multimode vibronic coupling effects in molecules. *Int. J. Quantum Chem.* **2009**, *20*, 251–267.
- (50) Petrenko, T.; Neese, F. Efficient and automatic calculation of optical band shapes and resonance Raman spectra for larger molecules within the independent mode displaced harmonic oscillator model. *Chem. Phys.* **2012**, *137*, No. 234107.
- (51) Szabo, A.; Ostlund, N. S. *Modern Quantum Chemistry: Introduction to Advanced Electronic Structure Theory*, 1st ed.; Dover Publications, Inc.: Mineola, 1996.
- (52) Klinkusch, S.; Tremblay, J. C. Resolution-of-identity stochastic time-dependent configuration interaction for dissipative electron dynamics in strong fields. *Chem. Phys.* **2016**, *144*, No. 184108.
- (53) Hermann, G.; Pohl, V.; Tremblay, J. C. An open-source framework for analyzing N-electron dynamics. II. Hybrid density functional theory/configuration interaction methodology. *J. Comput. Chem.* **2017**, *38*, 2378–2387.
- (54) Born, M.; Huang, K. *Dynamical Theory of Crystal Lattices*; Clarendon, Oxford, 1954.
- (55) Klinkusch, S.; Saalfrank, P.; Klamroth, T. Laser-induced electron dynamics including photoionization: A heuristic model within time-dependent configuration interaction theory. *Chem. Phys.* **2009**, *131*, No. 114304.
- (56) Dunning, T. H. Gaussian basis sets for use in correlated molecular calculations. I. The atoms boron through neon and hydrogen. *J. Chem. Phys.* **1989**, *90*, 1007–1023.
- (57) Coccia, E.; Mussard, B.; Labeye, M.; Caillat, J.; Taïeb, R.; Toulouse, J.; Luppi, E. Gaussian continuum basis functions for calculating high-harmonic generation spectra. *Int. J. Quantum Chem.* **2016**, *116*, 1120–1131.
- (58) Turney, J. M.; Simmonett, A. C.; Parrish, R. M.; Hohenstein, E. G.; Evangelista, F. A.; Fermann, J. T.; Mintz, B. J.; Burns, L. A.; Wilke, J. J.; Abrams, M. L.; et al. Psi4: an open-source ab initio electronic structure program. *Wiley Interdiscip. Rev.: Comput. Mol. Sci.* **2012**, *2*, 556–565.
- (59) Kratzer, A. The rotation spectrum of halogen hydrogens. *Z. Phys.* **1920**, *3*, 289–307.
- (60) Varshni, Y. P. Comparative Study of Potential Energy Functions for Diatomic Molecules. *Rev. Mod. Phys.* **1957**, *29*, 664–682.
- (61) Baranov, V.; Gribov, L.; Novosadov, B. Calculation of vibronic spectra of polyatomic molecules in the franck–condon and herzberg–teller approximations: Part I. Methods for calculating matrix elements. *J. Mol. Struct.* **1981**, *70*, 1–29.
- (62) Kaneshima, K.; Ninota, Y.; Sekikawa, T. Time-resolved high-harmonic spectroscopy of ultrafast photoisomerization dynamics. *Opt. Express* **2018**, *26*, 31039–31054.
- (63) Marston, C. C.; Balint-Kurti, G. G. The Fourier grid Hamiltonian method for bound state eigenvalues and eigenfunctions. *J. Chem. Phys.* **1989**, *91*, 3571–3576.
- (64) Sawada, R.; Sato, T.; Ishikawa, K. L. Implementation of the multiconfiguration time-dependent Hartree–Fock method for general molecules on a multiresolution Cartesian grid. *Phys. Rev. A* **2016**, *93*, No. 023434.